Mathematical and numerical evaluation of the damping behaviour for a multi-strand bar

Haval Asker[1], Jem Rongong[2], Charles Lord[3]
[1,2,3] *The University of Sheffield, Mechanical Department*

ABSTRACT

Multi-strand systems include, but are not limited to, electrical wire conductors, structural cables, and some composite reinforcements. These systems (apart from composite reinforcements) are generally metallic for a variety of reasons. One often overlooked advantage is that dry friction between metal contacts can provide damping over significantly wider temperature ranges than is typical for common damping materials such as viscoelastic polymers. This paper, proposes a mathematical model that describes the hysteretic vibrational behaviour of a frictionally constrained multi-strand bar constructed from strands that have a circular cross-section. The mathematical model analytically predicts the frictional system stiffness under simply supported boundary conditions. The assembled strands are numerically simulated using finite elements and hysteresis behaviour is compared to that obtained from the mathematical model. This shows that the mathematical model is capable of predicting the stiffness and the force-displacement hysteresis response of the system for a variety of conditions.

Keywords: *Vibration control, loss factor, friction, composite, high temperature.*

1. INTRODUCTION

Systems comprising dry friction contact can provide considerable amounts of damping over large operating temperature ranges. Energy dissipation from friction interfaces involving a small number of relatively large contact surfaces, such as turbine blade roots, has received significant research interest. On the other hand, damping from a large number of relatively small contacts, such as might be found in a multi-strand cable, is not nearly as well understood. There is therefore a need for efficient and accurate models to allow optimisation of this kind of damping mechanism in order to improve vibration control in mechanical systems. Practical examples of these systems are fibre bundles, suspension systems, woven fabrics, multi-stranded wire dampers, composite materials with dry frictional contact between the mating layers, and damaged/delaminated fibre composites.

Dry friction provides a nonlinearity within a system and therefore adds complexity. A considerable amount of work has been presented previously [1]–[10] which focus on introducing the associated frictional damping as an approximated equivalent viscous damping. The analytical models presented were compared to results from either numerical models, experimental data, or both demonstrating the usefulness and accuracy of this approach. Both empirical or semi-empirical models have been introduced [11], [12] That are dependent on unique parameters extracted from experimental data. A substantial amount of existing mathematical models describe multi-layered structures as either bonded or jointed layers [13]–[15] and ignore the frictional effect in the interface contact between the mating layers.

[1] PhD student, hkaasker2@sheffield.ac.uk
[2] Senior Lecturer, j.a.rongong@sheffield.ac.uk
[3] Lecturer, c.lord@sheffield.ac.uk

* Haval Asker

In this paper, the mathematical model developed includes the frictional effects by introducing them directly into the system stiffness. This does not depend on any empirical parameters other than material properties and the coefficient of friction. The interface of the un-bonded strands is allowed to slide against each other reducing the system stiffness as these structures, when sliding, have multi neutral axes. The results from the model are capable of defining the stick and sliding regions. A comparison between the mathematical model and numerical models using finite element (FE) analysis is made and good agreement is obtained

2. MATHEMATICAL MODEL

In this study, the system considered was a multi-strand bar comprising seven steel strands of circular cross-section, each one experiencing frictional contact with its neighbours. Two configurations were considered: one with 3 mm and the other with 4 mm diameter strands. The arrangement allowed for six strands to be placed radially around a core strand. Each of the outer strands was in contact with the adjacent outer strand and simultaneously with the core strand. This is depicted in Fig. 1.

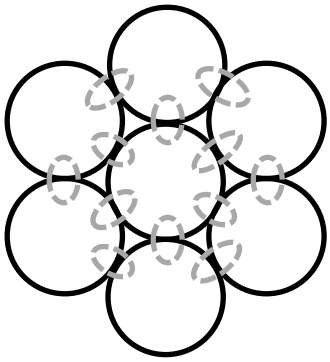

Figure 1 - Seven strand bar. Contact points are indicated by the 'dashed ovals'.

The contact condition between the mating surfaces has a direct effect on the overall system stiffness and its response. Therefore, it is essential to estimate the stiffness of the multi-stranded bar system in order to accurately describe the damping behaviour. The prediction of the frictional second moment of area for the multi-stranded bar is thought to be the prerequisite to estimating the system stiffness in the current study.

2.1 Frictional second moment of area

The stiffness of the system can be represented by the frictional second moment of area. The term "frictional second moment of area" in this paper refers to taking into consideration the friction effect with the second moment of area. When these systems are either bonded or frictionless, the second moment of area can be calculated using the parallel axis theorem as shown in Eq. (1),

$$I_{\mathrm{n}} = \sum_{1}^{\mathrm{n}} \left(I_{\mathrm{o}} + Ad^2 \right), \tag{1}$$

where I_n is the second moment of area for the system, I_0 is the second moment of area for an individual strand, A is the cross-section area, d is the transfer distance from the strand centre to the system geometrical centre and n is the number of involved strands.

For a bonded case, d is equal to the strand radius as shown in Fig. 2a. For a frictionless case, d is equal to zero (as shown in Fig.2b) as each strand has its own neutral axis and there is no transfer distance between the strand's neutral axis and the geometric centre of the system. For instance, in Fig. 2b there will be two separate systems. In a frictional case, d should increase with increasing the

coefficient of friction, μ, and the direction of this increment is towards the contact regions as shown in Fig. 2c.

For a case that the friction is involved between the mating strands, it is the authors' understanding that until now no equation has previously been formed that can describe this case. In this section, a mathematical method will be introduced to predict the frictional second moment of area at any magnitude of μ up to a limit of the equivalent of the strands being bonded. This is achieved firstly by estimating the deformation relationship with a range of μ magnitudes from frictionless contact and end with bonded contact. Second, the estimated deformation magnitudes are used to predict the frictional second moment of area at any specific μ magnitude.

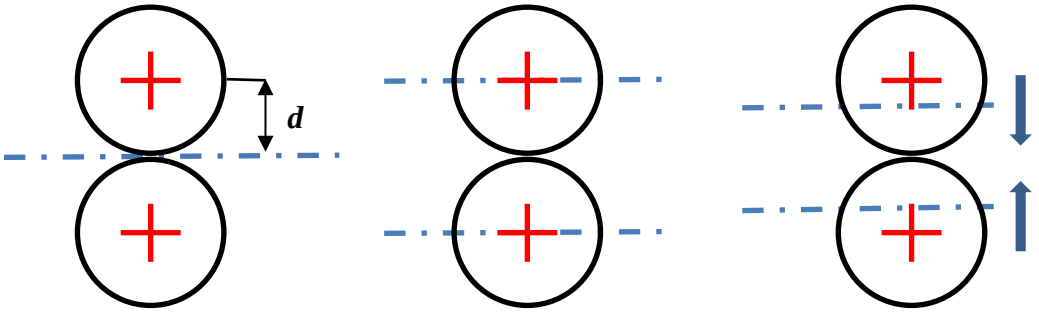

Figure 2 - Transfer distance, d, for strands that are (a) *bonded,* (b) *frictionless, and* (c) *frictional. Dashed lines represent the neutral axes.*

2.1.1 Effect of coefficient of friction, μ, on stiffness

To provide upper and lower bounds for the frictional second moment of area, two cases were considered: perfectly bonded and frictionless. Eq. (2) was used to calculate the second moment of area for a system with frictionless contact

$$I_{frictionless} = \frac{N\pi r^4}{4}, \tag{2}$$

where N is the number of strands involved in the system and r is the radius of the individual strands in the multi-strand bars system. Using Eq. (2), the total deformation in the system can be estimated from Eq. (3),

$$\delta_{frictionless} = \frac{F l^3}{48 E I_{frictionless}}, \tag{3}$$

where E is the modulus of elasticity, l is the span distance, and F is the applied force at the centre of l. For the bonded case, the second moment of area can be calculated by Eq. (4),

$$I_{bond} = \frac{55\pi r^4}{4}. \tag{4}$$

The total deformation can be calculated by the use of Eq. (5),

$$\delta_{bond} = \frac{F l^3}{48 E I_{bond}}. \tag{5}$$

To calculate the equivalent μ during the bonding case, a correlation at the contact between the strands for the shear stress and the frictional stress, from the frictional forces, is required. The shear stress is identified by Eq. (6), [16],

$$\tau_{shear} = \frac{3F}{I}\left[\frac{t^2}{4} - y_c{}^2\right], \tag{6}$$

where t is the total height for the multi-stranded bar, y_c is the distance from the body centre to the interfacial contact surface where the slip initiated and in a bonded contact the y_c is equal to zero. The friction stress is provided in Eq. (7),

$$\tau_{frictional} = \frac{F_c\,\mu}{A}, \tag{7}$$

where A is the contact area between two cylinders and can be found through Eq. (8) [17],

$$A = 2L\sqrt{\frac{8\left(2F_c + F\right)\frac{1-v^2}{E}}{\left(\frac{2\pi L}{r}\right)}}, \tag{8}$$

where v is Poisson's ratio.

Initiation of the sliding stage is when the shear stress is equal to the frictional stress and therefore, the μ between each strand can be calculated by Eq. (9),

$$\mu = \frac{3F\,A}{I_{bond}\,F_c}\left[\frac{t^2}{4} - y_c{}^2\right], \tag{9}$$

where F_c is the clamping force, I_{bond} is the second moment of area for a bonded case.

By knowing that μ in the frictionless contact is zero, a relationship can be plotted between the deformations, δ, and μ as shown in Fig. 3. This plot provides the magnitude of the δ at any specific μ between frictionless and bonded states. The corresponding δ for each μ can be used to calculate the related frictional second moment of area in Eq. (10),

$$I_{frictional} = \frac{F\,l^3}{48\,E\,\delta}. \tag{10}$$

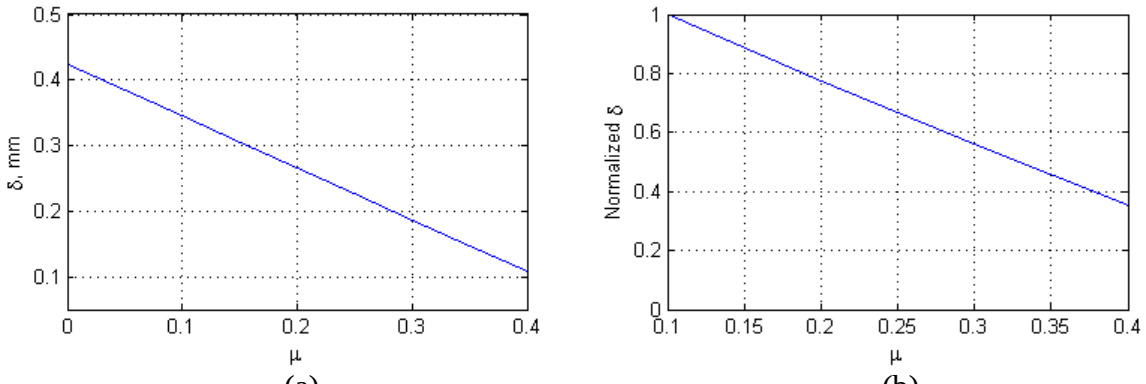

(a) (b)

Figure 3 - δ versus μ for (a) *mathematical model and* (b) FE *results.*

The relation between the deformation and the μ is near linear with R^2=X.

It is crucial to investigate the validity of this linear relationship therefore a FE model (described in Section 3) was compared in Fig. 3b. The FE model δ is normalised due to the model being from a slightly different set of parameters. From the FE results it is shown that the relationship tends to be near linear hence the relationship in the mathematical model can be considered acceptable.

Fig. 4 depicts the nonlinear behaviour of the second moment of area through frictionless, frictional and bonded stages. It is apparent the importance the frictional second moment of area has on the system stiffness through the different contact stages. In order to model a system with frictional behaviour, describing the stiffness accurately is essential.

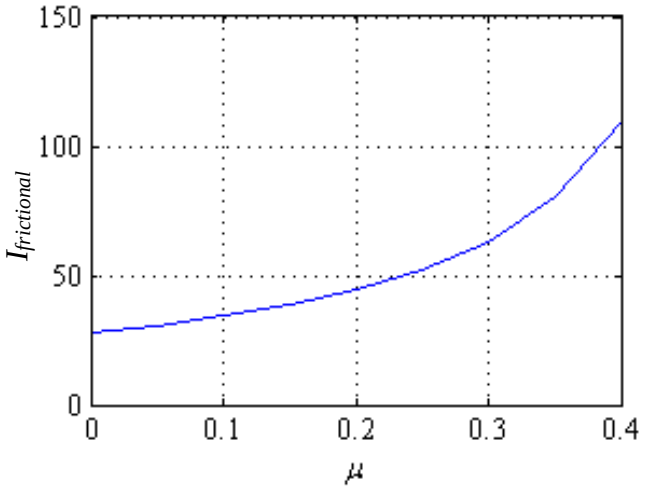

Figure 4 - Frictional second moment of area versus μ.

2.2 Sensitivity of the frictional second moment of area

FE models were used to demonstrate the effect of the μ on the system stiffness by creating force-displacement curves as shown in Fig. 5. The stick-slip part of the force-displacement curve is considered of an importance because it indicates the transition between bonding and sliding contact and how the second moment of area (or stiffness) changes. It is clearly shown the stick region, stick-slip region and the sliding region during the loading process in the multi-strand bar system with different individual strand diameters.

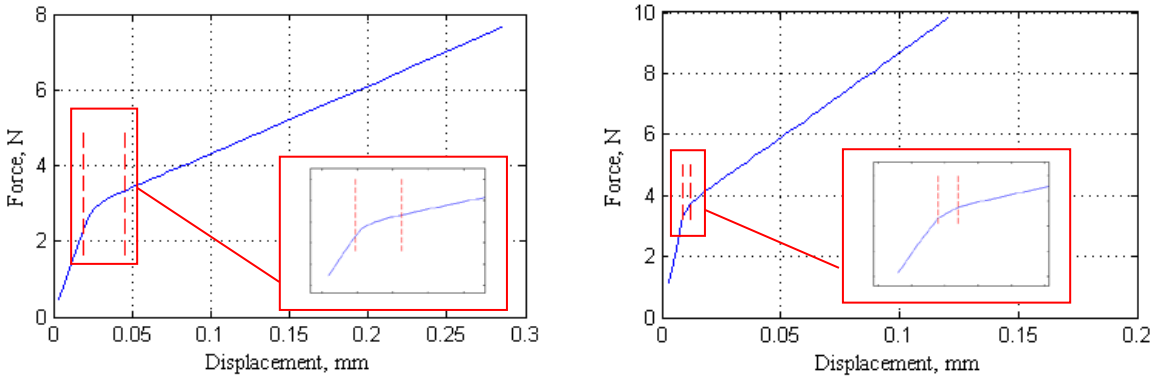

(a) (b)

Figure 5 - Stick-slip region (dashed lines indicate upper and lower bounds) of the multi-strand bar for strands of (a) 3mm *and* (b) 4mm.

The sensitivity of the frictional second moment of area, to the applied force was investigated through revealing the part where the stick-slip region lay as depicted in Fig. 6.

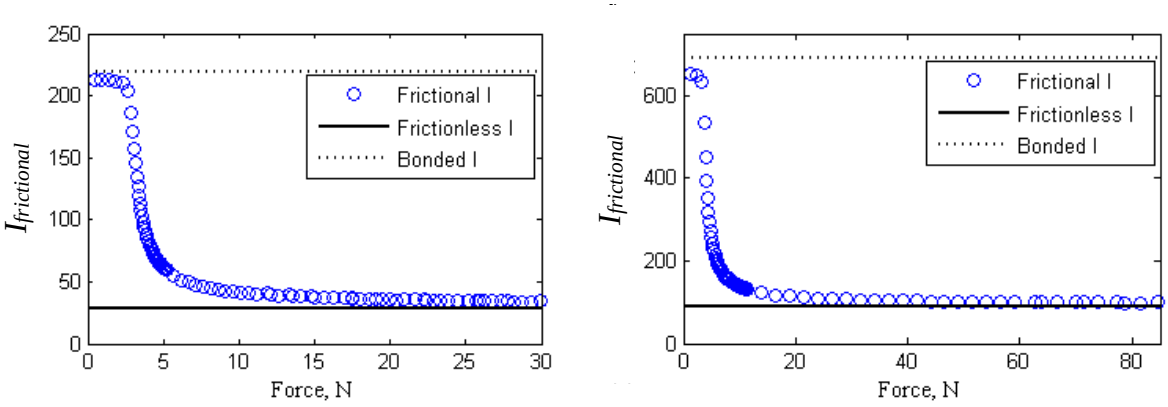

(a) (b)

Figure 6 - Sensitivity of the frictional second moment of area to the applied load for a multi-strand bar system with strands diameters for (a) *3 mm and* (b) *4mm.*

The transition of the frictional second moment of area from the sticking stage (dashed line) to the sliding stage (solid line) passing through the stick-slip stage is depicted clearly in Fig. 7.

2.3 Mathematical hysteresis loop

A mathematical model has been developed to describe the overall system stiffness of a multi-strand bar by accounting for the effect of friction. The model produces a force-displacement response. This can be extended into a force-displacement hysteresis loop to estimate the system loss factor.

Fig. 7 shows the various loading and unloading stages for the hysteresis loop. The starting point for the hysteresis loop begins from the origin point (0, 0) in the Cartesian coordinate system. Point (1, 1) presents the sliding stage and ends in point (1, 2).

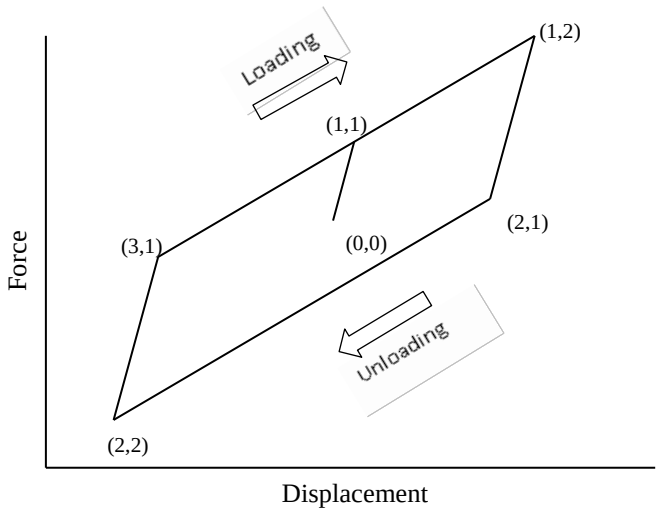

Figure 7 - Hysteresis loop stages

To estimate the force-displacement hysteresis loop, the shear stress between the mating strands and the frictional stresses at the contact regions can be used to estimate the force required to start the slipping in the multi-strand bar system. At the moment when the contacted strands begin to slide, the frictional force equals the shear force that tries to initiate the slipping. This force is described by Eq. (11) [18],

$$F_{slip} = F(1,1) = \frac{3F_c \mu I_{bond}}{A\left[\frac{z^2}{4} - y_c{}^2\right]}. \quad (11)$$

Eq. (12) is used to calculate the deformation resulting from that force,

$$\delta(1,1) = \frac{F_{slip} l^3}{48 E I_{bond}}. \quad (12)$$

The third stage starts from point (1, 2) and represents the maximum force and displacement applied on the system. In this stage, depending on the applied force, the resulting deformation is calculated by Eq. (13),

$$\delta(1,2) = \frac{F l^3}{48 E I_{frictional}}. \quad (13)$$

The fourth stage starts from point (2, 1) which is considered the start of the unloading stage. For this stage, Eqs. (14) and (15) calculate the force and deformation respectively.

$$F(2,1) = F - 2F_{slip} \quad (14)$$

$$\delta(2,1) = \frac{F(2,1) l^3}{48 E I_{frictional}} \quad (15)$$

The unloading stage ends at the point (2, 2). Eqs. (16) and (17) are used to calculate the force and deformation respectively.

$$F(2,2) = -F(1,2) \quad (16)$$

$$\delta(2,2) = -\delta(1,2) \quad (17)$$

The sliding starting between mating strands when the system transitions from the unloading to loading stage is represented between the end of the fourth stage (2, 2) and the start of fifth stage (3,1) which is calculated by the use of Eqs. (18) and (19).

$$F(3,1) = -F(2,1) \quad (18)$$

$$\delta(3,1) = -\delta(2,1) \quad (19)$$

2.4 Numerical models

FE models for a seven strand multi-strand bar were created to simulate the frictional behaviour. For the purpose of comparison, the FE models were supposed to mimic the mathematical models. Two sets of models were built with each strand length of 250mm but with different strand diameters of 3mm and 4mm. The types of elements used consisted of 3-D 20-node hexahedral (SOLID186), 8-node surface-surface contact (CONTA174) and target segment (TARGE170). The number of nodes was 70033 and 105176 for the models with individual bar diameters of 3mm and 4mm respectively. The modulus of elasticity used was 190GPa and between the strands and the contact it was assumed μ=0.25.

2.4.1 Boundary conditions and loadings

The boundary and loading conditions were applied to the FE models to match those applied in the mathematical model as simply supported. The clamping force was presented in the simulation as a radially distributed pressure [19] on the bars surface in the direction toward the centre strand as depicted in Fig. 8.

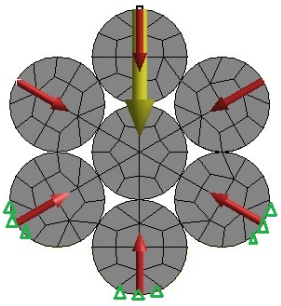

(a) (b)

Figure 8 - FE model for (a) *loads and boundary conditions and* (b) *for the seven strand bar under bending.*

The peak-to-peak displacement controlled loadings were 0.5mm, 1mm and 1.5mm. The clamp pressure was the ratio of the clamping forces to the area where the clamping forces was applied. The FE models were exposed to cyclic static flexural loading (ignoring transient effects) to obtain force-displacement hysteresis loops that were used to determine the system loss factor.

3 RESULTS AND DISCUSSION

Figs. 9 and 10 show the force-displacement hysteresis loops obtained both from the mathematical and FE models for the multi-strand bar system consisting of seven strands.

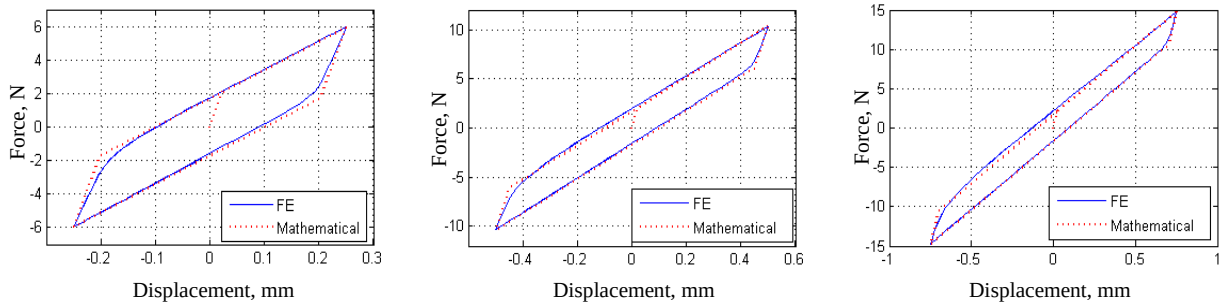

(a) (b) (c)

Figure 9 – Mathematical and FE model comparison for a 3mm diameter seven strand bar system for peak-to-peak displacements of (a) *0.5mm,* (b) *1.0mm, and* (c) *1.5mm.*

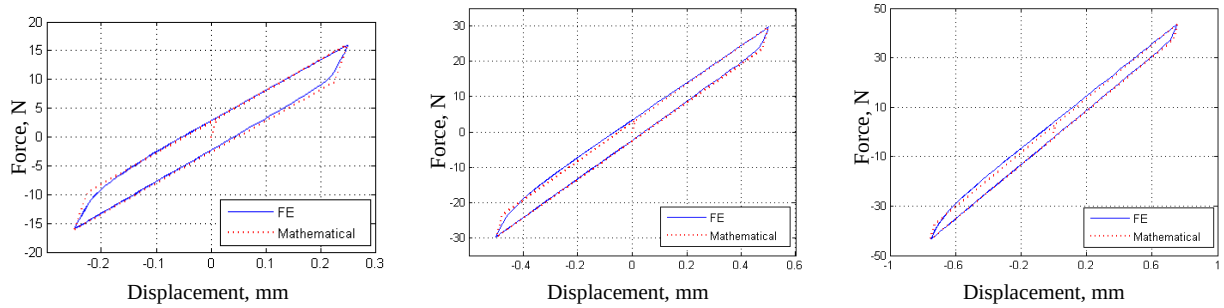

(a) (b) (c)

Figure 10 – Mathematical and FE model comparison for a 4mm diameter seven strand bar system for peak-to-peak displacements of (a) *0.5mm,* (b) *1.0mm, and* (c) *1.5mm.*

In the hysteresis loops obtained from the FE models, the lower edge presents the loading stage and the upper edge presents the unloading stage as the applied displacement started from zero to the maximum amplitude. For comparison purposes with the mathematically obtained hysteresis loops, the numerical results were re-centred to represent being loaded equally between the positive

and negative parts of the hysteresis loops, while in reality they had been loaded in the negative part only.

In the FE obtained hysteresis loops, and especially in Fig. 9, the transition between the loading and unloading stages has a nonlinear trend with a decrease in the system stiffness. This transition between the sticking and sliding is ignored by the mathematical model and replaced with a linear discontinuity. Although this is not accounted for, there is still a good correlation between the sticking and slipping regions.

In this study, the loss factor was decided to be an indicator for the damping levels in the system. The loss factor was compared between the mathematical and FE model results. The difference in loss factor is shown in Table 1.

Table 1: Difference in loss factor as a function of strand diameter and peak-to-peak displacement loads

Strand diameter	**Peak-to-peak displacement loads**		
(mm)	**0.5mm**	**1mm**	**1.5mm**
3	0.0%	0.3%	6.2%
4	9.0%	5.0%	12.0%

The frictional behaviour between the mathematical and FE model for the hysteresis loops compare well with one another. While the mathematical model mostly represents the loading and un-loading stages, it does was not represent the precise nonlinear behaviour for the stick-slip region. When the system is largely dominated by slipping, the stick-slip region carries minimal importance and the presented mathematical model is valid. Conversely, when the system is dominated by stick-slip, the proposed model loses its' accuracy.

4 CONCLUSIONS

Several conclusions can be drawn from the results obtained in this paper. The main conclusions are:

- The mathematical model provides an approximate prediction which follows the numerically-computed force-displacement response over most stages of loading and the un-loading.
- The relationship between the frictional second moment of area and the coefficient of friction is highly nonlinear.
- The transition region between the stick and slip stages plays an important role in changing the system stiffness from being bonded to frictional to being frictionless.
- The relationship between the system deformation and the coefficient of friction is linear.

ACKNOWLEDGEMENT

The authors acknowledge The University of Sheffield and the Higher Committee for Education Development in Iraq HCED for their support.

BIBLIOGRAPHY

[1] C. F. Beards, "The damping of structural vibration by controlled interfacial slip in joints," *J. Vib. Acoust. Stress Reliab. Des.*, vol. 105, no. 3, pp. 369–373, 1983.

[2] E. H. Dowell, "Component mode analysis of nonlinear and nonconservative systems," *J. Appl. Mech.*, vol. 47, pp. 172–176, 1980.

[3] E. H. Dowell and H. B. Schwartz, “Forced with response of a cantilever damper a dry friction attached , part ii : experiment,” *J. Sound Vib.*, vol. 91, no. 2, pp. 269–291, 1983.

[4] E. H. Dowell, “in an arbitrary mode are considered; also a pinned-pinned rectangular plate is studied. In all cases, a simple explicit formula is obtained,” vol. 105, pp. 243–253, 1986.

[5] E. H. Dowell, “Free vibrations of a linear structure with arbitrary support conditions,” *J. Appl. mechnaics*, vol. 38, pp. 595–600, 1971.

[6] L.Jezequel, “Structural damping by slip in joints,” *J. Vib. Acoust. Stress Reliab. Des.*, vol. 105, no. 81, pp. 497–504, 1983.

[7] T. K. Pratt and R. Williams, “Non-Linear analysis of stick / slip motion,” *J. Sound Vib.*, vol. 74, pp. 531–542, 1981.

[8] D. M. Tang and E. H. Dowell, “Damping in beams and plates due to slipping at the support boundaries, part 2: Numerical and experimental study,” *J. Sound Vib.*, vol. 108, no. 3, pp. 509–522, 1986.

[9] A. Zmitrowicz, “A vibration analysis of a turbine blade system damped by dry friction forces,” *Int. J. Mech. Sci.*, vol. 23, no. 12, pp. 741–761, 1981.

[10] C. Lord, J. Rongong, and A. Hodzic, “The use of layered composites for passive vibration damping,” in *29th IMAC, a Conference on Structural Dynamics. series 3*, 2011, pp. 289–298.

[11] M. Salehi, H. Heshmat, and J. F. Walton, “On the Frictional Damping Characterization of Compliant Bump Foils,” *J. Tribol.*, vol. 125, no. 4, pp. 804–813, 2003.

[12] J. Wojewoda, A. Stefański, M. Wiercigroch, and T. Kapitaniak, “Hysteretic effects of dry friction: modelling and experimental studies,” *Philos. Trans. R. Soc. London A Math. Phys. Eng. Sci.*, vol. 366, no. 1866, pp. 747–765, 2008.

[13] K. Asadi, H. Ahmadian, and H. Jalali, “Micro/macro-mlip damping in beams with frictional contact interface,” *J. Sound Vib.*, vol. 331, no. 21, pp. 4704–4712, Oct. 2012.

[14] W. Chen and X. Deng, “Structural damping caused by micro-slip along frictional interfaces,” *Int. J. Mech. Sci.*, vol. 47, no. 8, pp. 1191–1211, 2005.

[15] C. H. Menq, P. Chidamparam, and J. H. Griffin, “Friction damping of two-dimensional motion and its application in vibration control,” *J. Sound Vib.*, vol. 144, pp. 421–447, 1991.

[16] S. P. Goodier and J. N. Timoshenko, *Theory of elasticity*, Third edit. McGraw-Hill classic textbook reissue series. McGraw-Hill, 1970.

[17] K. L. Johnson, *Contact mechanics*. Cambridge University Press, 2004.

[18] C. Lord and J. Rongong, “A single layer constitutive model for the dynamics and vibration damping of layered built-up structures using microslip and macroslip models,” in *54TH AIAA/ASME/ASCE/AHS/ASC Structures, Structural Dynamics, and Materials Conference*, 2013, pp. 7374–7387.

[19] H. K. Asker, J. A. Rongong, and C. E. Lord, “Stiffness and loss factor of unbonded , multi-strand beams under flexural deformation,” in *International Conference on Engineering Vibration*, 2015, pp. 1518–1529.